Acta Oceanol. Sin., 2019, Vol. 38, No. 3, P. 60–71
https://doi.org/10.1007/s13131-019-1399-1
http://www.hyxb.org.cn
E-mail: hyxbe@263.net

A preliminary study on an upper ocean heat and salt content of the western Pacific warm pool region

Xiaoxin Yang[1, 2], Xiaofen Wu[1]*, Zenghong Liu[1], Chunxin Yuan[3]

[1] State Key Laboratory of Satellite Ocean Environment Dynamics, Second Institute of Oceanography, Ministry of Natural Resources, Hangzhou 310012, China

[2] Dalian Naval Academy, People's Libration Army, Dalian 116000, China

[3] College of Oceanic and Atmospheric Sciences, Ocean University of China, Qingdao 266100, China

Received 13 November 2017; accepted 28 December 2017

Abstract

On the basis of Argo profile data of the temperature and salinity from January 2001 to July 2014, the spatial distributions of an upper ocean heat content (OHC) and ocean salt content (OSC) of the western Pacific warm pool (WPWP) region and their seasonal and interannual variations are studied by a cyclostationary empirical orthogonal function (CSEOF) decomposition, a maximum entropy spectral analysis, and a correlation analysis. Probable reasons for variations are discussed. The results show the following. (1) The OHC variations in the subsurface layer of the WPWP are much greater than those in the surface layer. On the contrary, the OSC variations are mainly in the surface layer, while the subsurface layer varies little. (2) Compared with the OSC, the OHC of the WPWP region is more affected by El Niño-Southern Oscillation (ENSO) events. The CSEOF analysis shows that the OHC pattern in mode 1 has strong interannual oscillation, with eastern and western parts opposite in phase. The distribution of the OSC has a positive-negative-positive tripole pattern. Time series analysis shows that the OHC has three phase adjustments with the occurrence of ENSO events after 2007, while the OSC only had one such adjustment during the same period. Further analysis indicates that the OHC variations are mainly caused by ENSO events, local winds, and zonal currents, whereas the OSC variations are caused by much more complex reasons. Two of these, the zonal current and a freshwater flux, have a positive feedback on the OSC change in the WPWP region.

Key words: ocean heat content, salt content, the western Pacific warm pool, Argo data

Citation: Yang Xiaoxin, Wu Xiaofen, Liu Zenghong, Yuan Chunxin. 2019. A preliminary study on an upper ocean heat and salt content of the western Pacific warm pool region. Acta Oceanologica Sinica, 38(3): 60–71, doi: 10.1007/s13131-019-1399-1

1 Introduction

The western Pacific warm pool (WPWP) is a region with high temperature relative to its periphery, and is one of the main heat sources driving global atmospheric motion. Changes in this region would have great influence on the global atmosphere and oceans, so the WPWP has always been a research focus in the atmospheric and marine sciences. Before the 1980s, owing to limited on-site observation data of environmental elements of the atmosphere and oceans, researchers could not monitor numerous physical and oceanographic phenomena over the oceans reliably and provide timely warnings and forecasts. From 1985, a 10 year tropical ocean global atmosphere program (TOGA) was organized and carried out internationally, and a coupled ocean atmosphere research experiment (TOGA-COARE) (Yuter et al., 1995) was then conducted. In addition, a decade-long, global, quasi-synchronous observation starting from 1990 was done within a world ocean circulation experiment (WOCE) program (WOCE, 2003). During this period, most coastal states began to investigate special subjects and obtained many valuable and first-hand observational *in situ* data (Godfrey et al., 1998). On the basis of that, studies of popular marine topics, especially of the WPWP and its upper ocean heat content (OHC) and ocean salt content (OSC) began to emerge (including the relationships between warm pools and the distribution and variations of the upper OHC, plus relationships between the upper OHC and ocean atmosphere interactions such as the Kuroshio current and ENSO events.

Research has shown that in most large-scale ocean-atmosphere interactions over the Pacific, the upper OHC has greater sensitivity and interannual variations in comparison with the SST (Lin, 1990). Considering that China is not far from the WPWP region, upper OHC variations in such regions may have great influence on the country's climate change, because they may affect regional circulation patterns or intensity (Yu and Lin, 1997). Upper OHC anomalies have been widely used to study the dynamic process of the ENSO events. For example, regarding the upper OHC as one of the important predictors of the ENSO, scientists have proposed many theoretical models such as a "delayed oscillator model", a "western Pacific oscillator model", and a "charge–discharge oscillator model" (Suarez and Schopf, 1988; Weisberg and Wang, 1997; Picaut et al., 1997; Jin, 1997a, b; Wang, 2001). Chao (2001) found that positive and negative SST anom-

Foundation item: The National Natural Science Foundation of China under contract Nos 41406022 and 41606003; the Scientific Research Fund of the Second Institute of Oceanography, State Oceanic Administration of China under contract Nos JG1812 and JG1709; the Special Program for the National Basic Research of China under contract No. 2012FY112300.
*Corresponding author, E-mail: wuxiaofen83@163.com

alies causing El Niño/La Niña originate near the subsurface layer/thermocline of the warm pool region, and then spread eastward and upward along the thermocline in the equatorial region under certain atmospheric conditions. This results in the El Niño/La Niña events in a conventional sense, when they spread to the surface layer of the eastern equatorial Pacific (Chao, 2001). Successive studies indicated that westward-spreading SST anomalies in the north equatorial current region constitute an important mechanism causing abnormal SST variations in the WPWP, and advanced the concept of a cyclonic SST "signal channel" in the tropical Pacific (Zhang and Chao, 2002). Upper zonal current anomalies in the western and central equatorial Pacific are an important driver of the zonal movement of the OHC, influencing that movement 4–6 months in advance. The OHC variations in the WPWP region are also under the influence of climate change. With regard to the mechanism of such variations, it has been suggested that zonal wind stress anomalies in the middle equatorial Pacific are very important drivers of the zonal movement of the OHC in the WPWP region (Qi et al., 2010).

There is strong correlation between the ENSO events and the OSC variations on an intraannual time scale (Xie et al., 2009). Precipitation anomalies caused by the ENSO result in the OSC variations, and large OSC variations substantially change the thermohaline circulation, which inevitably strongly alters the heat flux and the global climate. Some research has reported that the influence of increasing OSC by 1 g/L in a certain temperature range on a water density is the same as that of decreasing temperature by 3–4°C (Broecker, 1991). The studies of OSC change mechanisms suggest that in open oceans, the great evaporation capacity in subtropical regions and heavy precipitation in the polar regions result in the OSC variations. Further, circulations influenced by wind, temperature, and other factors induce the horizontal transport of the OSC, which may be very rapid and powerful in the upper several hundred meters. Therefore, evaporation, precipitation, and transport by ocean currents constitute the main influences on the OSC distribution (Harvey, 1945).

Although the studies of the OHC in both China and abroad have had numerous achievements, the OHC estimation remains a major challenge. Various mapping schemes proposed for unobservable areas would create uncertainty in the OHC estimation (Palmer and Hanines, 2009; Lyman and Johnson, 2008), as would deviations from various observational instruments (especially deviations of XBT data during 1966–2000). In addition, selection of the climate state (the spatiotemporal resolution of ship observational data obtained in recent decades is not adequate to develop an effective climate state) also causes errors in the OHC analysis (Abraham et al., 2013). The situation of the OSC estimation is similar. Because large-area, historic profile data of the salinity are lacking, ocean assimilation data like SODA or fit underway observation data with uneven spatial and temporal distributions have generally been used in the studies of the OSC (Levitus, 1986). Furthermore, current studies generally take the integral of the salinity over volume, without considering the influence of the water density. As a result, there is still a long way to go in high-precision the OSC estimation and large-scale studies of the OSC distribution and its variation (Wu et al., 2001).

The implementation of a global Argo real-time ocean observing network in 2000 has brought a good opportunity for the high-precision estimation of a basin-scale OHC and OSC. Argo profiling floats can provide the temperature and salinity data of the global oceans in a depth range (0–2 000)×10^4 Pa with high spatiotemporal resolution, and had obtained 1×10^6 temperature and salinity profiles by early November 2007. The number of profiles is increasing constantly at 120 000 each year. The Argo network effectively complements information on the subsurface sea that satellites cannot obtain. Lyman et al. (2006) indicated that during the period 1955–2002, as observational methods improved, uncertainty in the OHC estimation minimized after implementation of the Argo program. Compared with all previous observing systems, the Argo ocean observing network can provide a more uniform space time data distribution for the studies on the global climate change. This is especially so for in-depth explorations of the relationships between the distribution and variations of upper OHC and OSC in the western Pacific region and the warm pools, ENSO and other oceanographic phenomena, and ocean atmosphere interactions (Xu et al., 2008). In addition, the network guarantees a bright future for more precise the upper OHC and OSC estimation, the exploration of seasonal and interannual OHC and OSC variations, the studies of the relationships between the OHC anomalies and the ENSO events on an interannual scale, and the ocean–atmosphere interaction. Therefore, this paper explores the spatial distribution of the OHC and particularly that in the WPWP region, plus their seasonal and interannual variations using new Argo profile data from 14 a.

2 Data and methodology

2.1 *Data description*

Monthly average temperature and salinity profile data from 2001 to 2014 that were used to calculate the OHC were extracted from a data set provided by the Japan Agency for Marine-earth Science and Technology. It is produced by merging many types of *in situ* observational data, but most are Argo profiling data (Fig. 1). This data set was available on a 1°× 1° grid for 25 pressure levels spanning (0–2 000)×10^4 Pa, with separate levels 10×10^4 Pa apart above the 150×10^4 Pa level and (20–100)×10^4 Pa apart below the 150×10^4 Pa level (Hosoda et al., 2008). The temperature and salinity profile data in the WPWP (20°S–30°N, 120°E–140°W, (0–120)×10^4 Pa) region were used.

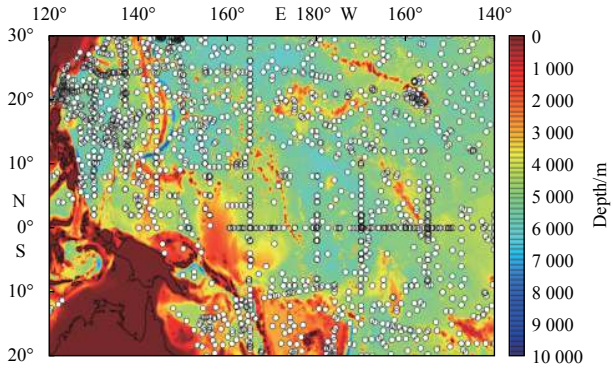

Fig. 1. Deployment locations of Argo floats in the study area from 2001 to 2014.

2.2 *Methodology*

The OHC and the OSC can be integrated in a vertical profile as

$$\mathrm{OHC} = \int_Z^0 c_\mathrm{p}\rho T \mathrm{d}z,$$

$$\mathrm{OSC} = 0.001 \int_Z^0 \rho S \mathrm{d}z,$$

where c_p is the specific heat of seawater at a constant pressure (c_p varies with the temperature and salinity); ρ is the seawater density; and dz is the vertical extent of the integration interval. The unit of the OHC is J/m^2 and that of the OSC is g/m^2; we assume OHC/OSC is uniform across each grid.

We also integrated the OHC and the OSC in a horizontal profile at various depths:

$$\mathrm{OHC_h} = \int \rho c_p T \mathrm{d}A\,,$$
$$\mathrm{OSC_h} = 0.001 \int \rho S \mathrm{d}A\,,$$

where A is the horizontal extent of the integration interval. After the integration, we calculated the average of the OHC and the OSC at 10×10^4 Pa, 50×10^4 Pa and 120×10^4 Pa, and researched yearly variations of their averages after standardization. In this situation, the unit of the average OHC is J/m^3 and that of the average OSC is g/m^3.

Given evidence that many signals in geophysical data are cyclostationary (Kim and Gerald, 1997; Kim and Wu, 1999; Kim and Cheng, 2001), we introduced the concept of a cyclostationary empirical orthogonal function (CSEOF) analysis to capture time-varying spatial patterns (LV component) and longer-time scale fluctuations (PC component) present in geophysical signals. The significant difference between the CSEOF and EOF analyses is LV time dependence, which allows the spatial pattern of each CSEOF mode to vary in time (Figs 5 and 7). The temporal evolution of the spatial pattern of the CSEOF LVs is constrained to be periodic with a selected "nested period". That may be expressed as

$$T(\vec{r},t) = \sum\nolimits_i PC_i(t)\, LV_i(\vec{r},t)\,,$$
$$LV_i(t) = LV_i(t+d)\,,$$

where r and t represents spatial and temporal fields respectively, d is the nested period, an empirical number. Here we take d=12 because the period of the time series in the first mode of the EOF analysis is approximately 12 months. The advantages of the CSEOF analysis are that it can minimize mode mixing (a common problem in a EOF decomposition) and can account for both high and low frequency components of the annual cycle, and it does not require removal of the annual signal.

3 Basic features of OHC and OSC in WPWP region

3.1 *Characteristics of SST and SSS during ENSO events*

The WPWP is usually noted for its high temperature (SST> 28°C) and low salinity (SSS<35). Figure 2 shows locations of the 28.5°C isotherm and 34.8 isohaline at the surface (10×10^4 Pa) during the ENSO events. The eastern boundary of the isotherm expands substantially eastward during warm events and shrinks westward during cold events, with a double-tongue pattern. The north tongue is around 6°N with a longitudinal extent of 30°, and the south tongue is near 10°S with much smaller extent (about 15°). The trough of the double tongue was over the equator. Observational and modeling results indicate that such interannual displacements of the eastern edge of the warm pool are mainly attributable to the zonal advection associated with local wind forcing and its Kelvin and Rossby wave response (Picaut et al., 1996; Clarke et al., 2000). The northern and southern boundaries of the WPWP do not exhibit remarkable shifts during the ENSO cycle.

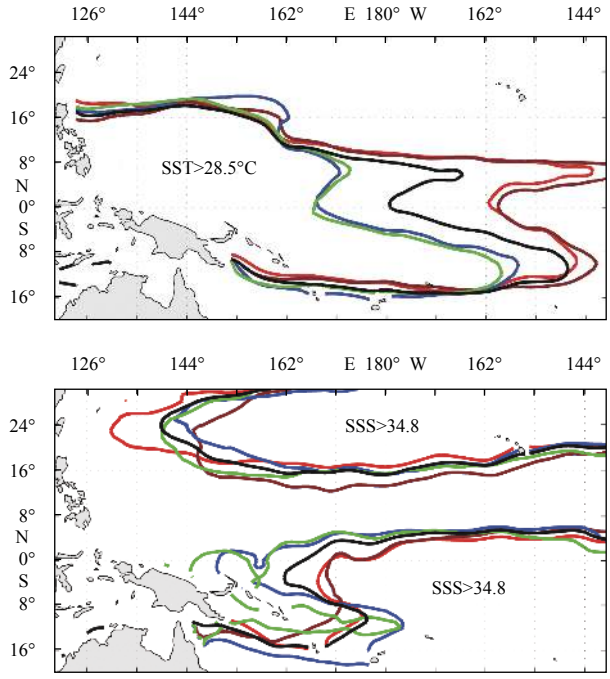

Fig. 2. Positions of 28.5°C isotherms (a) and 34.8 isohalines (b) at 10×10^4 Pa during ENSO events. The red line and yellow line denote El Niño, the blue line and green line denote La Niña, and the black line denotes neutral phase.

The isohaline does not change much in the ENSO events, especially east of the date line. However, in the southwest, there are complex changes that may be caused by heavy precipitation and transport from strong currents near the equatorial convergence zone (Delcroix et al., 1996; Reverdin et al., 1994).

3.2 *OHC and OSC variations at standard levels*

Figure 3 shows yearly variations of area-average OHCs at standard levels. The OHC on the sea surface varies as a sine function with period approximately 1 a and tended to be uniform during 2001–2007. It fluctuated strongly after 2007, during which there were two intermediate cold events (2007/2008 and 2010/2011 La Niña) and one intermediate warm event (2009/2010 El Niño) (Zhang and Weng, 1999). The amplitudes of area-average OHC variations on the subsurface were larger than those in the surface layer, and the OHC in the upper layer near the thermocline in the equatorial Pacific Ocean showed the interannual variability that was positively correlated with the El Niño events; the former usually leads the latter. Such a result is consistent with earlier studies (Chao et al., 2003; Pu et al., 2003). That is, an increasing number of works found that the subsurface ocean frequently had much greater and more stable changes. Finally, we conclude that the OHC at each standard level during the ENSO years had very different variabilities than the neutral years. The greatest change was usually around the 120×10^4 Pa layer, and the OHC change in the subsurface was opposite that on the surface layer. This may be related to the fact that abnormal signals in the ENSO cycle were first found in the subsurface ocean of the western Pacific and then moved eastward along the thermocline (Chao et al., 2003).

The annual variations of the area-average OSCs at standard

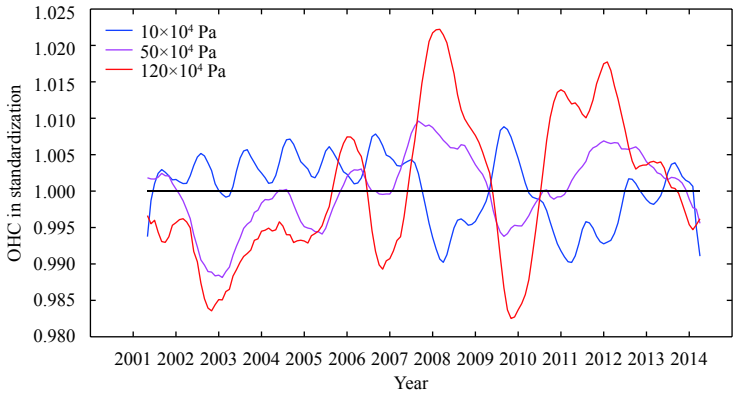

Fig. 3. Yearly variations of area-averaged OHCs at 10×10⁴ Pa, 50×10⁴ Pa and 120×10⁴ Pa.

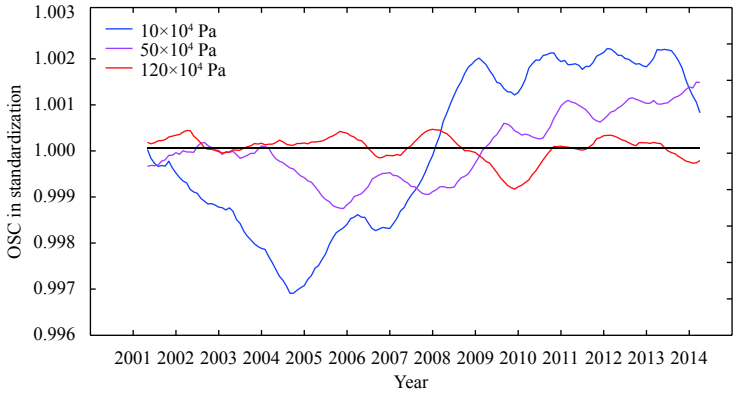

Fig. 4. Yearly variations of area-averaged OSCs at 10×10⁴ Pa, 50×10⁴ Pa and 120×10⁴ Pa.

levels were simple. Almost all trends exhibited a short-term climatic change (Fig. 4). In contrast with the OHC, the OSC on the surface had greater change than that in the subsurface, i.e., the amplitudes of the OSC variations decreased from the surface to subsurface ocean. Further, the OSC grew substantially after 2007 and maintained large values between 2009 and 2013.

4 CSEOF analysis

4.1 *OHC*

The first mode of the OHC variations in the WPWP had a zonal dipole pattern with see-saw anomalies in the western and eastern parts. The variance contributions of the first three modes are 46.57%, 10.91% and 8.26%. The sum of the first two modes' feature vectors is 57.49%, i.e., there were two tongue-shaped, large-value variation areas. One was in the region 0°–12°N, 130°–155°E with axis at approximately 8°N and the other was east of the date line with its axis around the equator. Maximum absolute values in the two areas were basically the same. This zonal antiphase pattern of the variations indicates that when the OHC of the west part of the WPWP increased, the OHC of the east part decreased, and vice versa. Figure 4 shows the spatial distribution of the OHC in the WPWP in the depth range (0–120)×10⁴ Pa (January–December).

Seasonal OHC variations also had this zonal antiphase feature. The amplitude maximized in winter (November through February) and minimized in summer (May through August). In winter, the maximum absolute values in both variation areas increased (i.e., the amplitude increased) and the areas enlarged, with the west area expanding eastward and the east area expanding westward. In summer, the maximum absolute values in both variation areas decreased and the areas shrank, the west area toward the west and the east area toward the east.

Figure 5 shows the time series of the first mode obtained by the CSEOF analysis. As seen from that figure and Fig. 4 (spatial anomaly field), when the time series maximized, the spatial anomaly field was large in the east and small in the west. At the trough, the field was large in the west and small in the east. This indicates that the OHC of the WPWP region in the depth range (0–120)×10⁴ Pa had three phase adjustments after 2007. Because this mode resembles the spatial structure of the ENSO, it may have a relationship with it. In addition, from a maximum entropy spectral analysis, the time series of the first mode show a significant period of 3 a.

4.2 *OSC*

As revealed by the CSEOF analysis of the OSC, the variance contributions of the first three modes are 33.14%, 21.96%, and 10.43%. The sum of the first two modes' feature vectors is 55.1%. Figure 6 shows the first mode's distribution in the WPWP region at depths (0–120)×10⁴ Pa as revealed by the CSEOF method (January–December). It is seen from the figure that the OSC distribution in the WPWP roughly had a positive–negative–positive tripole pattern from south to north. Two positive variation areas were northwest and south of the study area, and a negative variation area was between 18°N and 8°S. The latter area expanded gradually from west to east and extended to the northeast and southeast, almost spanning the entire tropical Pacific. In addition,

there were two extreme value centers in the negative variation area, one southwest of the equator and the other around 12°N. As seen from the upper OSC variations (January–December) in the WPWP region, the seasonal OSC variations also had this tripole pattern. The amplitudes of variation of the OSC were stronger in winter and spring (January through April), and weaker in summer and autumn (September through December). In winter and spring, the two maximum absolute values in the negative variation area maximized. The south extreme value center gradually extended southeast to 144°W, and its maximum absolute value and area of the center declined. The northeast extreme value center extended southeast and slightly east, oscillating east of the date line. The amplitudes in the north and south positive variation areas maximized in winter and spring, and minimized in summer and autumn. The coverage of the north positive variation area changed little with season, but the location of its extreme value center moved to the south in winter and spring, and to the north in summer and autumn. The south positive variation area expanded to the northwest in winter and spring, and shrank to the southeast in summer and autumn.

Figure 8 shows the time series of the first mode in the OSC variations. As seen from Figs 6 and 7 (spatial anomaly field), when the time series reaches its peak, the spatial anomaly of the OSC was large in both the north and south, and small in the middle. When it drops into the trough, the field is large in the middle and small in both the north and the south. The time series also show that OSC of the WPWP region only had one phase adjustment after 2007. In addition, an analysis via a maximum entropy spectral method showed that the OSC variations had significant period of 3 a.

5 Discussion

As revealed by the above analyses, both OHC and OSC of the WPWP had obvious interannual variations with a major period of 3 a, plus obvious seasonal variations. With regard to the latter, the spatial fields of the OHC and the OSC had different change patterns, with the OHC presenting a zonal dipole pattern and the OSC a tripole pattern. Previous studies have suggested that the temporal change of the OHC is balanced by net oceanatmosphere heat flux and heat advection (convergence/divergence). Many studies (e.g., Cayan, 1992; Kelly, 2004; Moon and Song, 2013; Wu et al., 2015; Wang et al., 2012) showed that surface fluxes contribute more to the OHC variation on a seasonal time scale, whereas the horizontal convergence and divergence of heat contributes more on longer time scales. The main causes of the OSC variations include local precipitation, horizontal advection, vertical convection, and others (Delcroix et al., 1998) on various time scales. In addition, both OHC and OSC are influ-

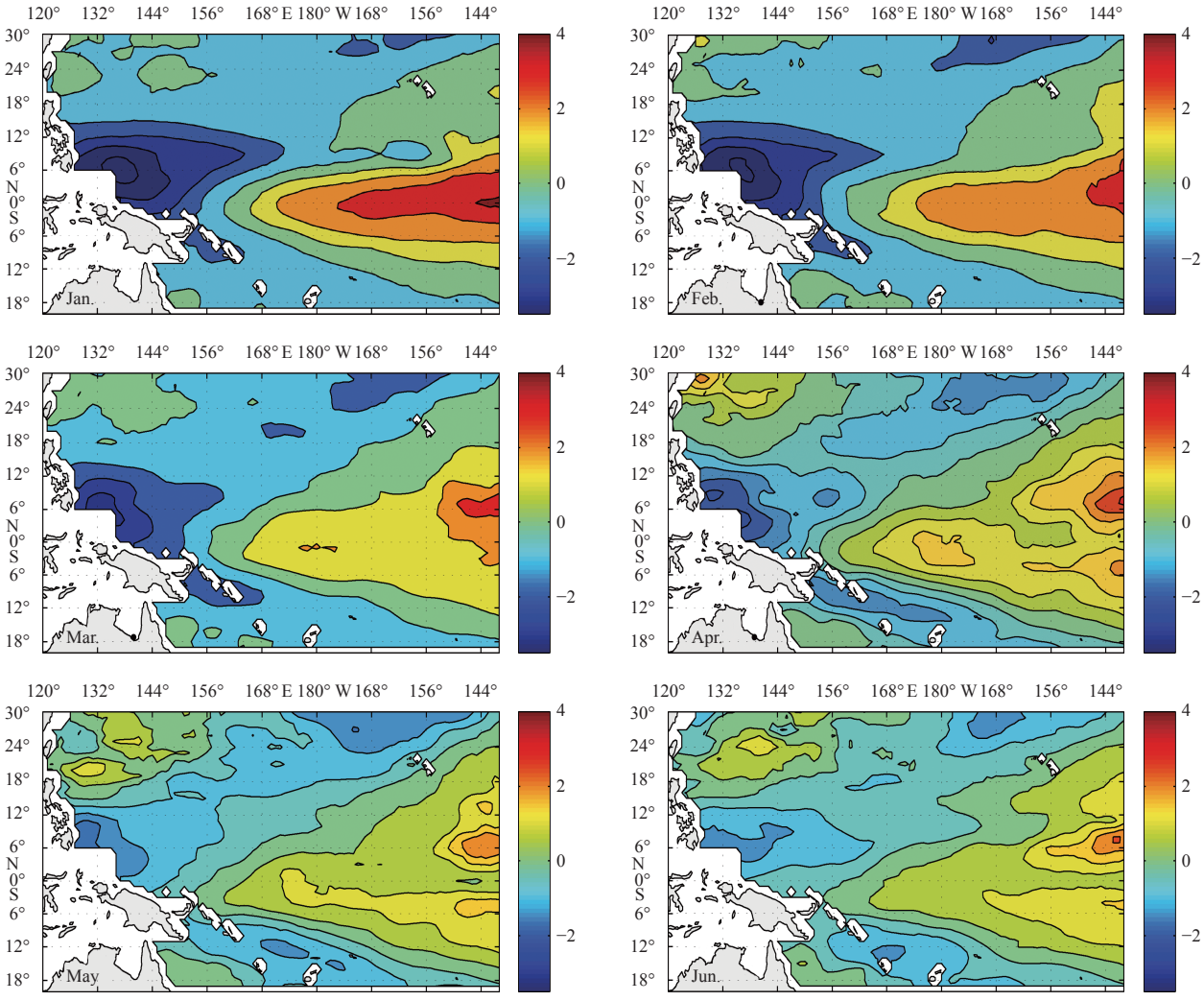

Fig. 5.

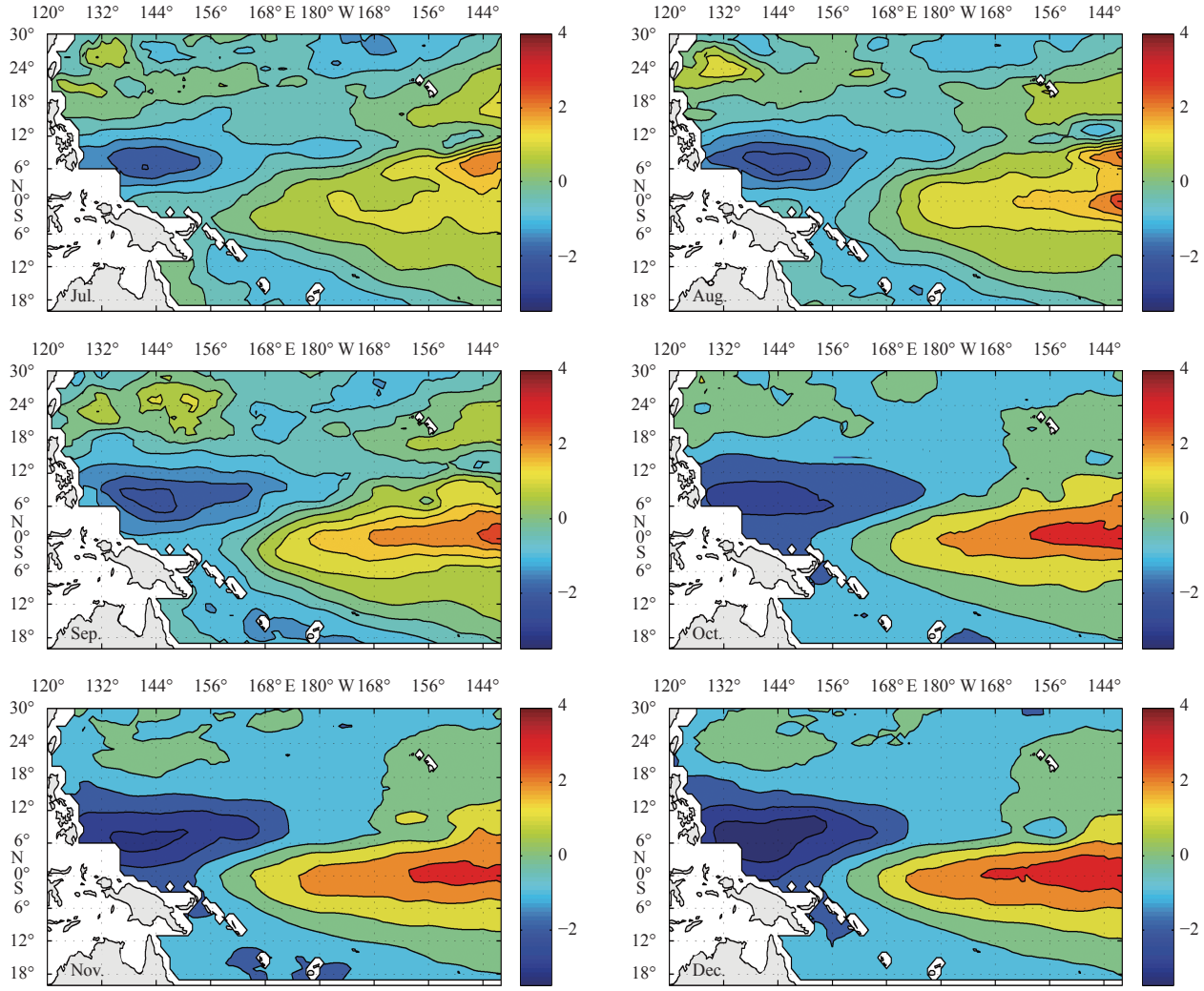

Fig. 5. Spatial patterns of CSEOF Mode 1 for OHC (January–December).

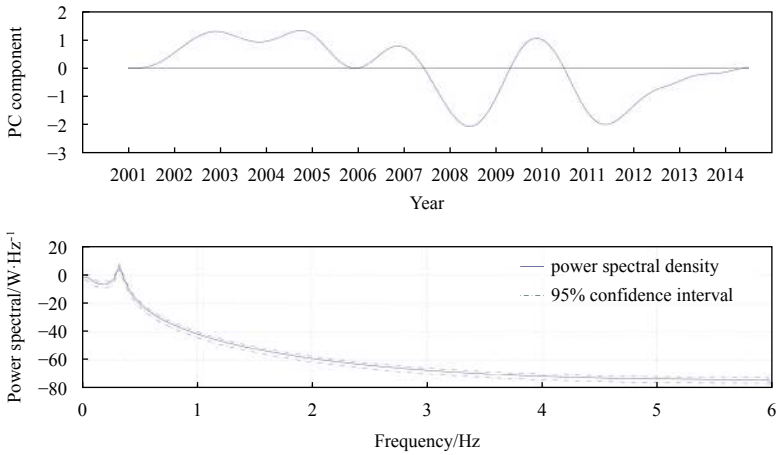

Fig. 6. Time series of CSEOF Mode 1 of OHC and its maximum entropy spectral analysis. PC component shows the weight of the spatial mode (LV component) varied with time.

enced by the ENSO events (Zhang and Weng, 1999; Xie et al., 2009). Here, we simply focus on the contributions of the wind-induced zonal advection and current advection. For deeper understanding, we should quantify each part's contributions to the OHC and OSC variations, a task in our future work.

5.1 *Probable causes of OHC variations*

As is well-known, the main period of the ENSO is 3–7 a. During the El Niño, the water temperature in the middle and eastern equatorial Pacific increases, while that of the western Pacific decreases. The situation during the La Niña is opposite. The ENSO

events have a major influence on large-scale climate changes around the world. The Niño3.4 index is one of the parameters reflecting the ENSO cycles. To discover possible relationships between the OHC interannual variations and ENSO events, we analyzed the relationship between the Niño3.4 index and the time series of the OHC in the WPWP region (Fig. 9).

It is shown in Fig. 9 that the two time series have very similar trends, and their correlation coefficient is 0.73 (passing the significance test with a confidence level of 0.05). After combining the time series with the spatial pattern of the first mode, we see that during the El Niño (as in 2010), the eastern part of the WPWP (overlapping with the Niño3.4 region, i.e., 5°S–5°N, 120°–170°W) had the positive OHC anomalies, indicating an increased OHC. The western part had the negative anomalies, indicating the decreased OHC. The situation during the La Niña (as in 2007/2008) is opposite. Studies have shown that the positive and negative SST anomalies during the ENSO originate from the subsurface layer in the area around the warm pool, then spread eastward and upward along the thermocline in the equatorial region under certain atmospheric conditions. This results in the El Niño/La Niña events in the conventional sense when they spread to the surface layer of the eastern equatorial Pacific (Chao, 2001).

The upper OHC variations are affected by ocean–atmosphere net heat flux and advection. By calculating the regional correlation coefficient between the net heat flux through the ocean surface and the time series of the first mode from the CSEOF analysis of the OHC, we determined that the large-value zone of the coefficient (R>0.4 and R<–0.4) between the two was mainly between 10°N and 10°S. This indicates that the area whose OHC is greatly affected by the net heat flux through the ocean surface is mainly in the equatorial zone. Many other studies (Cayan, 1992; Kelly, 2004; Moon and Song, 2013) have suggested that the impact of the net heat flux through the ocean surface on the OHC is mainly on a seasonal scale, whereas the advection has a more important effect on OHC interannual variations. Therefore, we focused on the contribution of the heat advection.

As studies have suggested, westerly wind anomalies excite motions in the equatorial wave guide that depress the thermocline in the east, reduce equatorial upwelling, and enhance eastward transport of warm surface waters from the western Pacific (Cane and Zebiak, 1985). The wind-forced zonal advection is important in the thermodynamics of the WPWP on interannual time scales (McPhaden and Picaut, 1990). At the initial stage of the El Niño, there is a positive temperature anomaly in the subsurface layer of the WPWP. With the burst of westerly winds, this anomaly spreads eastward along the thermocline in the equatorial region. Because the thermocline in the Pacific is oblique from east to west, the temperature anomaly spreads from the subsurface

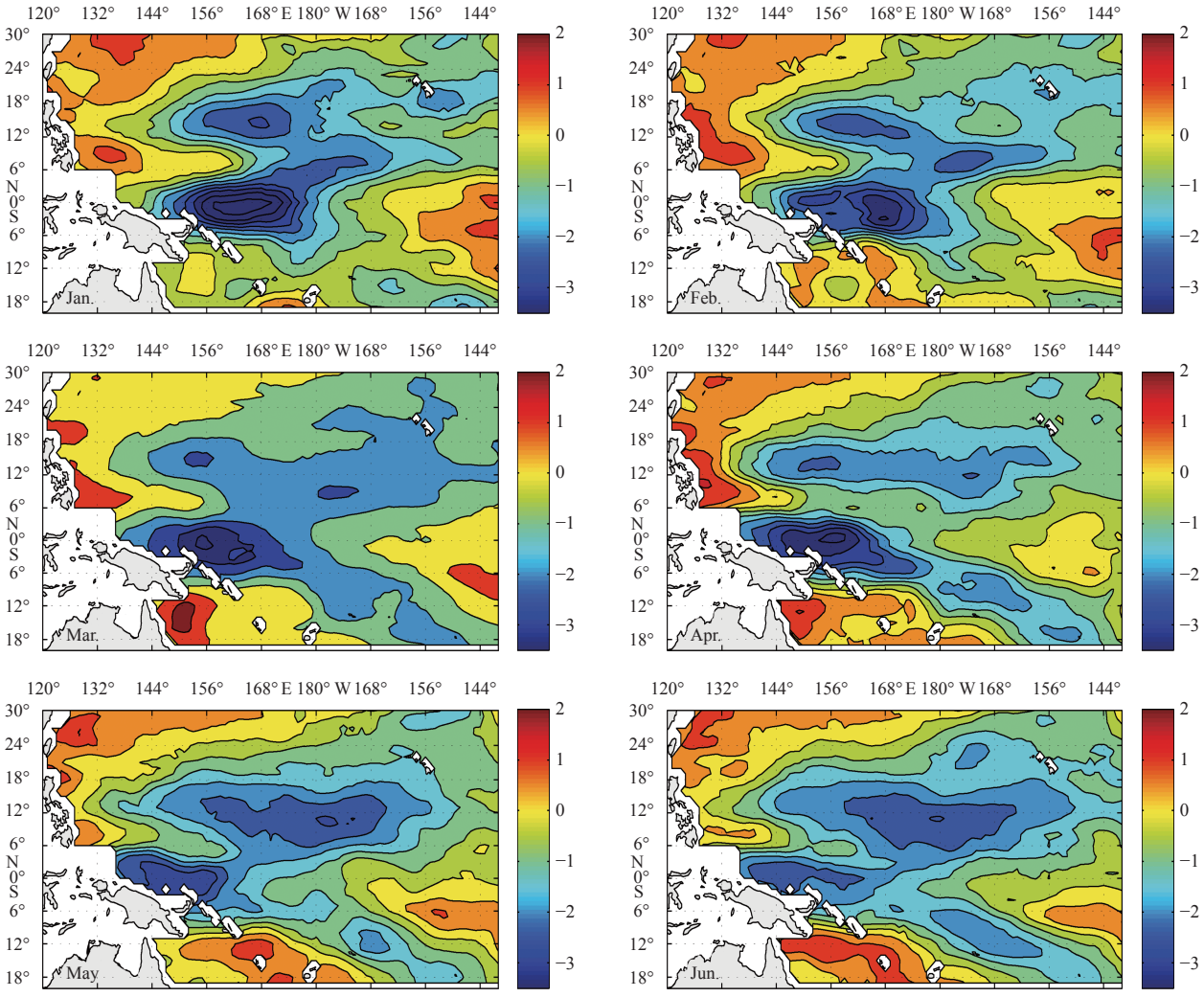

Fig. 7.

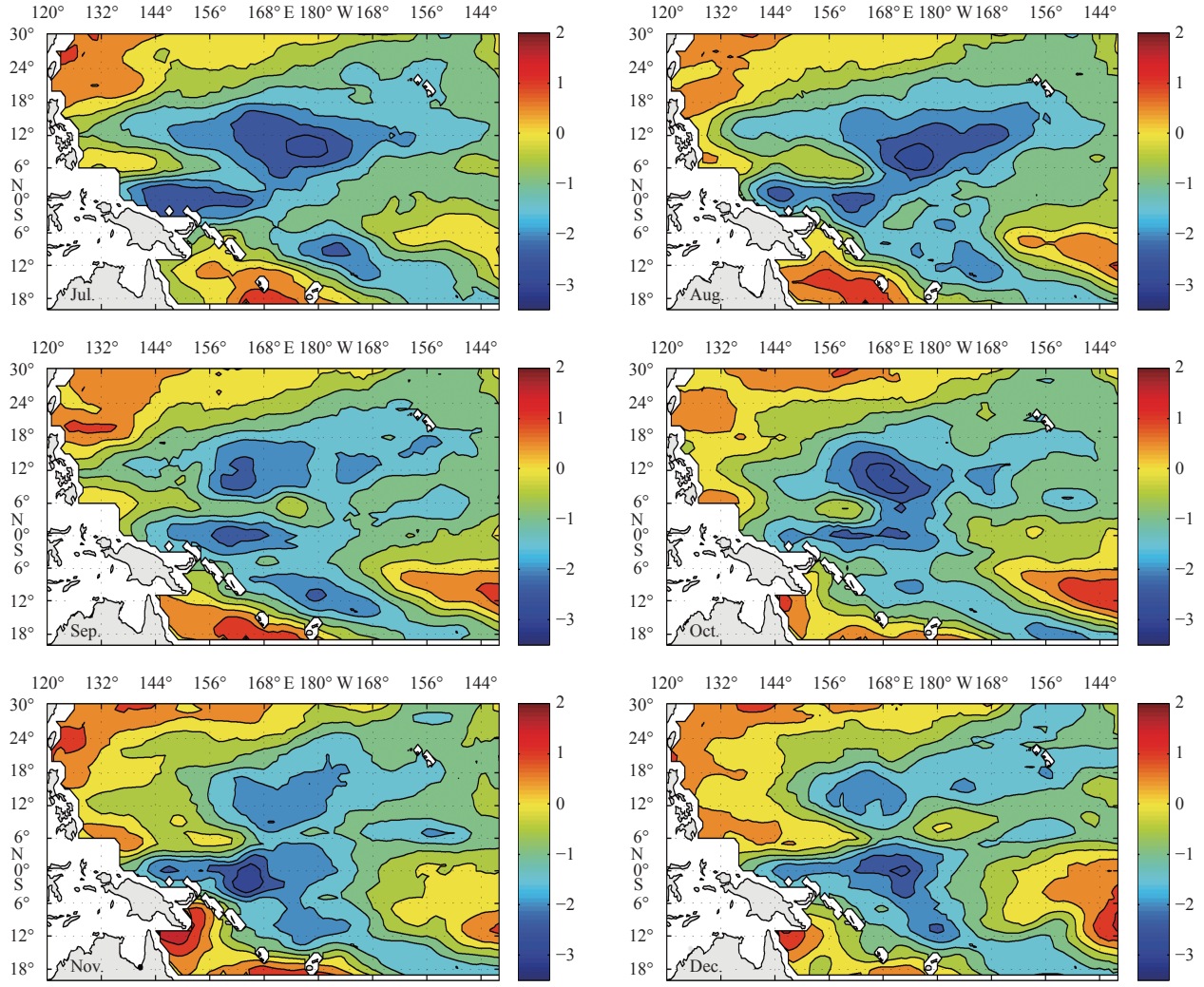

Fig. 7. Spatial patterns of CSEOF Mode 1 for OSC (Janaury–December).

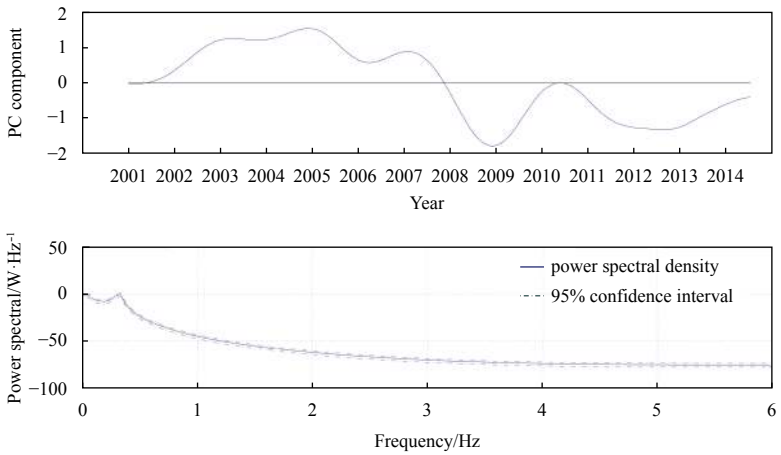

Fig. 8. Time series of CSEOF Mode 1 of OSC and its maximum entropy spectral analysis. PC component shows the weight of the spatial mode (LV component) varied with time.

layer of the western Pacific (120–200 m) to the near-surface layer of the eastern Pacific (20–60 m), resulting in an ENSO event. Afterward, this temperature anomaly spreads from east to west along the channel between 10° and 20°N (Mu and Li, 2000), laying the foundation for the next El Niño/La Niña as it reaches to the western Pacific. That is, the temperature anomaly in the subsurface layer of the Pacific circulates between the eastern and western Pacific, and there is a strong correlation between this temperature anomaly spread and zonal wind anomalies in the western Pacific. Therefore, it is reasonable to state that the OHC

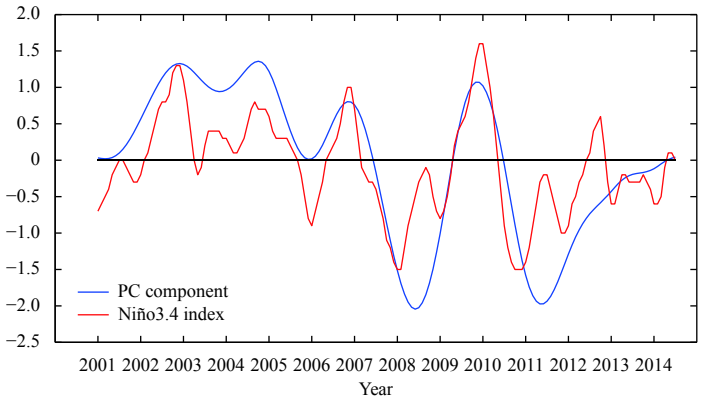

Fig. 9. Time series of CSEOF Mode 1 of OHC (blue) and Niño3.4 index (red). PC component shows the weight of the spatial mode (LV component) varied with time.

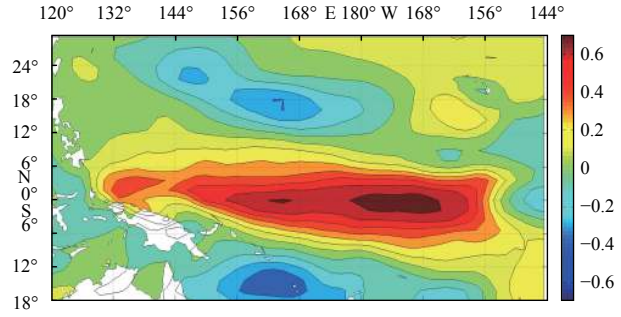

Fig. 10. Correlation of time series between CSEOF Mode 1 and zonal wind.

variations are induced by the ENSO through the wind forcing and the ocean current advection. This also explains why the spatial pattern of the first mode of the OHC has a zonal antiphase pattern that resembles the spatial structure of the ENSO.

Figure 10 shows time series correlation between the first mode from the CSEOF analysis of the OHC and zonal wind anomalies. As shown, the large-value area of the correlation coefficient between the two is mainly within the equatorial zone, where the correlation is positive. The maximum correlation (R>0.6) is over 5°S–5°N and 177°E–165°W. The correlation between the two is weakly negative in subtropical areas.

Figure 11 shows the OHC transport by the zonal currents ($Q_{\mathrm{OHC}} = \int \mathrm{OHC} \times \vec{U}\mathrm{d}z$; $Q_{\mathrm{OSC}} = \int \mathrm{OSC} \times \vec{U}\mathrm{d}z$) and the time-varying condition. The OHC transport corresponded well with the NEC, the NECC, and the SEC (Wu et al., 2015). The time series shows that during the El Niño, the OHC of the WPWP was mainly transported eastward, with the opposite pattern during the La Niña. This is consistent with the aforementioned OHC distribution with a positive anomaly in the east during El Niño and in the west during the La Niña. It is thus concluded that the zonal current and the zonal wind may be influences on the interannual OHC variations.

5.2 *Probable causes for OSC variations*

Studies on the change mechanism of the salt content at basin scale are very limited. However, studies of the salt content at smaller scales found that ocean current and the freshwater flux through the ocean surface are the two main causes of the OSC

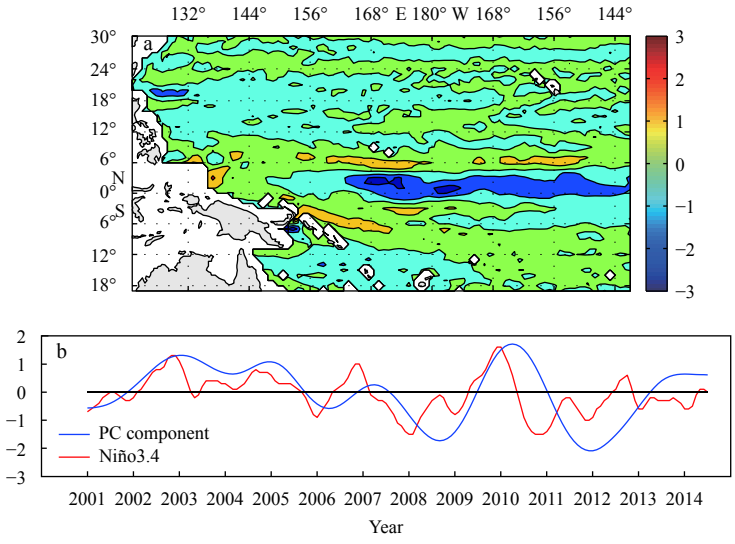

Fig. 11. Monthly average of spatial distributional pattern of CSEOF 1 (a), time series of CSEOF 1 (in blue) and Niño3.4 index (in red) (b). PC component shows the weight of the spatial mode (LV component) varied with time.

variations (Delcroix et al., 1998). Our OSC data were obtained by an integral calculation over depth, so the influence of the vertical currents is not addressed in this paper. One study (Gouriou and Delcroix, 2002) suggested that the upper OSC variations in the convergence belt of the southern Pacific are the strongest (that study also reveals that this is the main OSC variation area). Because the freshwater flux through the ocean surface in the study area is mainly dependent on precipitation, the following addresses possible mechanisms resulting in the OSC variations mainly from two aspects: zonal current and precipitation, which are controlled by the ENSO. This is done to explore possible relationships between the OSC and the ENSO cycle.

Because there have been few studies of the OSC, possible mechanisms resulting in upper OSC variations were explored by referring to previous studies. Delcroix et al. (1996, 1998) indicated that around the convergence belt of the southern Pacific, the salinity front of the WPWP divides low-salinity water in the tropical Pacific from high-salinity water, but the interannual displacement of the front is caused by precipitation changes induced by changes of the ascending branches of the Walker and Hadley circulations above the convergence belt of the southern Pacific during the ENSO. This results in the interannual variations of the sea surface salinity distribution (Gouriou and Delcroix, 2002). The interannual variations of the zonal currents may also influence that distribution by the convergence and the divergence. For example, in the latitudinal band of 17°S, the zonal currents are westward to the east of 175°E, and they are eastward west of that longitude. The convergence of the zonal currents as in this pattern could strengthen the salinity front. Therefore, the zonal current anomalies may also alter the sea surface salinity distribution. A westward anomaly of the zonal current speed would be 2–3 months earlier than westward movement of the salinity front, and an eastward anomaly of zonal current speed would be consistent with eastward movement of the salinity front. Under the influence of various factors, the salinity front in the southwest tropical Pacific would move westward and the salinity front in the equatorial Pacific would move eastward during the El Niño, The situation during the La Niña would be opposite. Therefore it is also reasonable to consider that the OSC variations are induced by the ENSO through precipitation and ocean current advection.

The OSC transport by the zonal currents was investigated (figure not shown). OSC was mainly transported westward from March through August by the NEC. There was also weak eastward transport around the NECC and the SEC, but the transport capacity was small. The westward transport by the NEC decreased substantially from September through January. The eastward transport by the NECC and the SEC increased slightly and maximized in December, but the transport capacity was still much smaller than the maximum capacity of westward transport in summer. During the El Niño, the OSC in the WPWP region was mainly transported westward, with the opposite situation during the La Niña. One study suggests that a westward geostrophic current in the western Pacific is intensified during the El Niño (Delcroix et al., 1998). As seen from Figs 6 and 7, the OSC distribution in the WPWP region (specifically, during both the 2009/2010 El Niño and 2010/2011 La Niña events) generally had a negative–positive–negative tripole pattern. That is, the OSC of the north and south parts of the WPWP region continued decreasing, while the OSC of the middle and west parts continued increasing. The amplitudes of the increases in the middle and west regions were different over the years. For example, the amplitude of the OSC increase in 2007/2008 was greatly reduced, while that amplitude during the El Niño in 2010 was relatively large. The above analysis indicates that though the influence of the zonal currents is limited, it still has a positive feedback on the OSC.

The interannual variations of the freshwater flux in the WPWP region were further analyzed (Fig. 12). The time series of the first mode from the EOF analysis for freshwater flux shows that it is 6 months ahead of the OSC, and its correlation coefficient is the maximum, at –0.71. As seen from Fig. 11, the largest variation area of freshwater flux was in the middle of the WPWP region, presenting a negative–positive–negative tripole pattern, similar to that of the OSC. A positive anomaly of the freshwater flux means that a sea area is losing water, and a negative anomaly means the opposite. By combining the pattern and time series of the fresh water flux, we found that OSC increase in the central part of the study area, and the decrease in the northwest and south parts that occurred 6 months later, lost freshwater and the latter gained freshwater. It can thus be inferred that the sea sur-

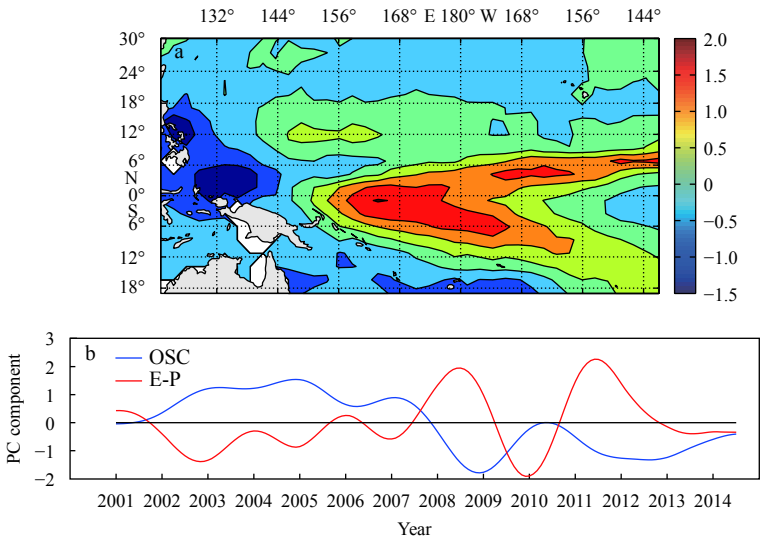

Fig. 12. Spatial pattern and temporal component of Mode 1 in the EOF analysis for sea surface fresh water flux. PC component shows the weight of the spatial mode (LV component) varied with time.

face freshwater flux may also have a positive feedback effect on the OSC.

6 Conclusions

On the basis of Argo data, spatiotemporal variation of the upper OHC and OSC in the WPWP region was studied using the CSEOF and spectral analysis plus other methods. The probable mechanisms for the variations were addressed, and the following results were obtained.

(1) The OHC variations in the subsurface layer of the WPWP region are much greater than those in the surface layer. On the contrary, the OSC variations are mainly in the surface layer, with the subsurface layer having little OSC variation. Compared with the OSC, the OHC in the WPWP region is more affected by the ENSO events.

(2) There are significant seasonal and interannual variations of the upper OHC and OSC in the WPWP region, and the main periods of their interannual variations are both 3 a. The spatial distribution of the OHC's first mode has an oscillating pattern, with the east and west parts opposite to each other in phase. The OSC distribution has a positive–negative–positive tripole pattern. The time series analysis shows that the OHC has three phase adjustments after 2007, which were related to the ENSO events. The OSC only had one phase adjustment during the same period.

(3) The OHC variations in the WPWP are closely correlated with the ENSO events. During the El Niño, the OHC in the east part of the WPWP increases, while that in the west part decreases. The situation during the La Niña was opposite. In addition, the OHC in the WPWP is affected by local wind and zonal current.

(4) The zonal current anomalies and the freshwater flux anomalies have a positive feedback effect on the OSC in the WPWP region.

Acknowledgements

We are grateful to those who generously provided data: the Japan Marine-earth Science and Technology Center (JAMSTEC) for the MOAA GPV Argo data, the US National Oceanic and Atmospheric Administration (NOAA) for the OSCAR data, the CMAP data and the Niño3.4 index. Besides, we thank the Computing Center of the State Key Laboratory of Satellite Ocean Environment Dynamics for calculation support (SOED-HPCC). We thank Steven Hunter from Liwen Bianji, Edanz Group China, for editing the English text of a draft of this manuscript.

References

Abraham J P, Baringer M, Bindoff N L, et al. 2013. A review of global ocean temperature observations: Implications for ocean heat content estimates and climate change. Reviews of Geophysics, 51(3): 450–483, doi: 10.1002/rog.20022

Broecker W S. 1991. The great ocean conveyor. Oceanography, 4(2): 79–89, doi: 10.5670/oceanog

Cane M A, Zebiak S E. 1985. A theory of El Niño and the Southern Oscillation. Science, 228(4703): 1085–1087, doi: 10.1126/science.228.4703.1085

Cayan D R. 1992. Latent and sensible heat flux anomalies over the northern oceans: driving the sea surface temperature. Journal of Physical Oceanography, 22(8): 859–881, doi: 10.1175/1520-0485(1992)022<0859:LASHFA>2.0.CO;2

Chao Jiping. 2001. New understandings of the development of El Niño and La Niña events. Bulletin of the Chinese Academy of Sciences , 16(6): 412–417

Chao Jiping, Yuan Shaoyu, Chao Qingchen, et al. 2003. The origin of warm water mass in warm pool subsurface of the western tropical Pacific—The analysis of the 1997–1998 El Niño. Chinese Journal of Atmospheric Sciences , 27(2): 145–151

Clarke A J, Wang Jianguo, van Gorder S. 2000. A simple warm-pool displacement enso model. Journal of Physical Oceanography, 30(7): 1679–1691, doi: 10.1175/1520-0485(2000)030<1679:ASWPDE>2.0.CO;2

Delcroix T, Gourdeau L, Hénin C. 1998. Sea surface salinity changes along the Fiji-Japan shipping track during the 1996 La Niña and 1997 El Niño period. Geophysical Research Letters, 25(16): 3169–3172, doi: 10.1029/98GL02320

Delcroix T, Henin C, Porte V, et al. 1996. Precipitation and sea-surface salinity in the tropical Pacific Ocean. Deep Sea Research: Part I. Oceanographic Research Papers, 43(7): 1123–1141, doi: 10.1016/0967-0637(96)00048-9

Godfrey J S, Houze R A Jr, Johnson R H, et al. 1998. Coupled ccean-atmosphere response experiment (COARE): an interim report. Journal of Geophysical Research: Oceans, 103(C7): 14395–14450, doi: 10.1029/97JC03120

Gouriou Y, Delcroix T. 2002. Seasonal and ENSO variations of sea surface salinity and temperature in the South Pacific Convergence Zone during 1976–2000. Journal of Geophysical Research: Oceans, 107(C12): 8011

Harvey H W. 1945. Recent Advances in the Chemistry and Biology of Sea Water. Britain: Cambridge University Press, 164

Hosoda S, Ohira T, Nakamura T. 2008. A monthly mean dataset of global oceanic temperature and salinity derived from Argo float observations. JAMSTEC Report of Research and Development, 8: 47–59, doi: 10.5918/jamstecr.8.47

Jin Feifei. 1997a. An equatorial ocean recharge paradigm for ENSO: Part I. Conceptualmodel. Journal of the Atmospheric Sciences, 54(7): 811–829, doi: 10.1175/1520-0469(1997)054<0811:AEORPF>2.0.CO;2

Jin Feifei. 1997b. An equatorial ocean recharge paradigm for ENSO: Part II. A stripped-down coupled model. Journal of the Atmospheric Sciences, 54(7): 830–847, doi: 10.1175/1520-0469(1997)054<0830:AEORPF>2.0.CO;2

Kelly K A. 2004. The relationship between oceanic heat transport and surface fluxes in the western north Pacific: 1970–2000. Journal of Climate, 17(3): 573–588, doi: 10.1175/1520-0442(2004)017<0573:TRBOHT>2.0.CO;2

Kim K Y, Cheng C L. 2001. On the evolution of the annual cycle in the tropical Pacific. Journal of Climate, 14(5): 991–994, doi: 10.1175/1520-0442(2001)014<0991:OTEOTA>2.0.CO;2

Kim K Y, Gerald R N. 1997. EOFs of harmonizable cyclostationary processes. Journal of the Atmospheric Sciences, 54(19): 2416–2427, doi: 10.1175/1520-0469(1997)054<2416:EOHCP>2.0.CO;2

Kim K Y, Wu Qigang. 1999. A comparison study of EOF techniques: analysis of nonstationary data with periodic statistics. Journal of Climate, 12(1): 185–199, doi: 10.1175/1520-0442-12.1.185

Levitus S. 1986. Annual cycle of salinity and salt storage in the world ocean. Journal of Physical Oceanography, 16(2): 322–343, doi: 10.1175/1520-0485(1986)016<0322:ACOSAS>2.0.CO;2

Lin Chuanlan. 1990. Some features of heat content changes of the oceanic upper layer in northwest Pacific during 1964–1982. Journal of Tropical Oceanography , 9(2): 78–85

Lyman J M, Johnson G C. 2008. Estimating annual global upper-ocean heat content anomalies despite irregular in situ ocean sampling. Journal of Climate, 21(21): 5629–5641, doi: 10.1175/2008JCLI2259.1

Lyman J M, Willis J K, Johnson G C. 2006. Recent cooling of the upper ocean. Geophysical Research Letters, 33(18): L18604

McPhaden M J, Picaut J. 1990. El Niño-Southern Oscillation, displacement of the western equatorial Pacific warm pool. Science, 250(4986): 1385–1388, doi: 10.1126/science.250.4986.1385

Moon J H, Song Y T. 2013. Sea level and heat content changes in the western north Pacific. Journal of Geophysical Research: Oceans, 118(4): 2014–2022, doi: 10.1002/jgrc.20096

Mu Mingquan, Li Chongyin. 2000. Interactions between subsurface ocean temperature anomalies in the western Pacific warm pool and ENSO cycle. Chinese Journal of Atmospheric Sciences, 24(4): 447–460

Palmer M D, Hanines K. 2009. Estimating oceanic heat content

change using isotherms. Journal of Climate, 22(19): 4953–4969, doi: 10.1175/2009JCLI2823.1

Picaut J, Ioualalen M, Menkes C, et al. 1996. Mechanism of the zonal displacements of the pacific warm pool: implications for ENSO. Science, 274(5292): 1486–1489, doi: 10.1126/science.274.5292.1486

Picaut J, Masia F, Penhoat Y. 1997. An advective-reflective conceptual model for the oscillatory nature of the ENSO. Science, 277(5326): 663–666, doi: 10.1126/science.277.5326.663

Pu Shuzhen, Yu Fei, Hu Xiaomin, et al. 2003. Spatial and temporal variability of heat content above the thermocline in the tropical Pacific Ocean. Acta Oceanologica Sinica, 22(2): 179–190

Qi Qinghua, Hou Yijun, Zhang Qilong. 2010. Zonal wind stress and current anomalies in equatorial Pacific Ocean and the zonal displacement of western Pacific warm pool. Oceanologia et Limnologia Sinica , 41(3): 469–476

Reverdin G, Frankignoul C, Kestenare E, et al. 1994. Seasonal variability in the surface currents of the equatorial Pacific. Journal of Geophysical Research, 99(C10): 20323–20344, doi: 10.1029/94JC01477

Suarez M J, Schopf P S. 1988. A delayed action oscillator for ENSO. Journal of the Atmospheric Sciences, 45(21): 3283–3287, doi: 10.1175/1520-0469(1988)045<3283:ADAOFE>2.0.CO;2

Wang Chunzai. 2001. A unified oscillator model for the El Niño-Southern Oscillation. Journal of Climate, 14(1): 98–115, doi: 10.1175/1520-0442(2001)014<0098:AUOMFT>2.0.CO;2

Wang Fan, Hu Dunxin, Mu Mu, et al. 2012. Structure, variations and climatic impacts of ocean circulation and the warm pool in the tropical Pacific Ocean. Advances in Earth Science , 27(6): 585–602

Weisberg R H, Wang Chunzhi. 1997. A western Pacific oscillator paradigm for the El Niño-Southern Oscillation. Geophysical Research Letters, 24(7): 779–782, doi: 10.1029/97GL00689

WOCE. 2003. WOCE observations 1990–1998; a summary of the WOCE global data resource. WOCE International Project Office, WOCE Report No. 179/02. WOCE, Southampton, UK, 4–48

Wu Xiaofen, Liu Zenghong, Liao Guanghong, et al. 2015. Variation of Indo-Pacific upper ocean heat content during 2001–2012 revealed by Argo. Acta Oceanologica Sinica, 34(5): 29–38, doi: 10.1007/s13131-015-0664-1

Wu Xiaofen, Xu Jianping, Zhang Qilong, et al. 2001. A preliminary study on upper ocean heat content of tropical western Pacific. Marine Forecasts (in Chinese), 28(4): 76–86

Xie Qiang, Li Haiyang, Wang Dongxiao. 2009. Interannual variations of salt content in the tropical Pacific Ocean. Advances in Marine Science (in Chinese), 27(2): 155–165

Xu Jianping, Liu Zenghong, Sun Chaohui, et al. 2008. Entire achievement of global Argo real-time ocean observing network. Ocean Technology (in Chinese), 27(1): 68–70

Yu Shuqiu, Lin Xuechun. 1997. Climatic jump of north pacific SST and its effect on precipitation of floods season in China. Journal of Tropical Meteorology (in Chinese), 13(3): 265–275

Yuter S E, Houze Jr R A, Smull B F, et al. 1995. TOGA COARE aircraft mission summary images: an electronic atlas. Bulletin of the American Meteorological Society, 76(3): 319–328, doi: 10.1175/1520-0477(1995)076<0319:TCAMSI>2.0.CO;2

Zhang Renhe, Chao Jiping. 2002. Some new aspects in understanding of ENSO cycle. Climatic and Environmental Research (in Chinese), 7(2): 175–183

Zhang Qilong, Weng Xuechuan. 1999. Analysis of heat content of the tropical western Pacific warm pool. Plateau Meteorology (in Chinese), 18(4): 584–589